PHYSICAL REVIEW C VOLUME 2, NUMBER 3 SEPTEMBER 1970

Elastic Scattering of 30.3-MeV Polarized Protons from ^{58}Ni, ^{120}Sn, and ^{208}Pb†

G. W. Greenlees
Rutherford High Energy Laboratory, Chilton, Didcot, England, and Department of Physics, University of Minnesota, Minneapolis, Minnesota 55455
and
V. Hnizdo, O. Karban, and J. Lowe
Department of Physics, University of Birmingham, Birmingham, England
and
W. Makofske
Department of Physics, University of Minnesota, Minneapolis, Minnesota 55455
(Received 2 April 1970)

Results are presented for the elastic scattering of 30.3-MeV polarized protons from targets of ^{58}Ni, ^{120}Sn, and ^{208}Pb. The angular region from 10 to 165° is covered with an absolute accuracy in the polarization measurements of about 0.01. The data, together with corresponding differential cross-section data previously reported, are analyzed using the optical model. Two forms of the model are used: (1) the standard version with independent geometries and ten parameters; and (2) the folding version of Greenlees, Pyle, and Tang with eight parameters. Good fits to the data are obtained, particularly for ^{208}Pb. Evidence is presented to support the suggestion that such models are most satisfactory for large nuclei (^{208}Pb), and that for smaller nuclei (^{120}Sn and ^{58}Ni) second-order corrections ignored in the model are playing a nonnegligible role.

I. INTRODUCTION

The elastic scattering of low- and medium-energy protons by atomic nuclei has been studied quite extensively in recent years. Such data are, in general, well represented by an optical-model description. The recent analysis of Becchetti and Greenlees[1] gives results which are characteristic of analyses of this type. This work simultaneously analyzed a large majority of the data available with $A > 40$ and $E < 50$ MeV, and examined a variety of possible A and E dependence of the model parameters. Such an analysis illustrates the predominance of differential cross-section data and the relative scarcity and inaccuracy of polarization and reaction cross-section data; no triple-scattering data of any sort were available.

A somewhat different approach to the analysis of elastic scattering data has been taken recently by Greenlees, Pyle, and Tang[2] (GPT). This approach attempts to express the real parts of the optical-model potential (central, isospin, and spin-orbit) in terms of nuclear nucleon density distributions and components of the two-body force. In Ref. 2 some accurate elastic differential-cross-section data were examined in considerable detail with encouraging results. The formalism of this approach was given in Ref. 2, but the analysis presented there involved some additional assumptions affecting the isospin and spin-orbit terms. These assumptions were of a minor nature and were invoked to reduce the computation periods involved in the analysis. An analysis using the complete model has recently been published.[3]

The work of Ref. 2 concentrated on the Rutherford Laboratory 30.3-MeV proton elastic differential cross-section data of Ridley and Turner,[4] since these were considered to be some of the most accurate and detailed of the data available. Corresponding polarization data were also available[5]; unfortunately this was for a somewhat lower mean energy (29.0 MeV) because of the necessity of using relatively thick targets with the low-intensity polarized beams in order to obtain acceptable counting rates. This difference in energy between the two types of data proved to be significant to the model and, coupled with the relatively large errors in the polarization data, resulted in the conclusions of the analyses resting almost entirely on the differential cross-section data.

One of the features of the GPT approach is that the geometries of the real parts of the potential are unambiguously related to each other and to nuclear nucleon distributions via the two-body force. In particular, the spin-orbit potential geometry cannot be treated independently from the real central geometry as is the case in standard optical-model treatments. Since the polarization angular distributions predicted by optical models are much more sensitive to the spin-orbit term in the potential than are the differential cross sections, it is important to have polarization data available in

order to obtain detailed information about this term and, in particular, to check the correlation with the real central term implied in Ref. 2.

The Mark-II polarized source of the Rutherford Laboratory proton linear accelerator has a figure of merit (P^2I) approximately 200 times better than the value for the Mark-I source used in the work of Ref. 5. This development enables much-improved polarization data to be obtained at the same energy (30.3 MeV) as the differential cross-section data of Ridley and Turner. The present paper is a report of such experiments together with an analysis of the data. Attention was concentrated on obtaining comprehensive and accurate data for a few typical elements. An angular range from 10 to 165° was studied for ^{58}Ni, ^{120}Sn, and ^{208}Pb; the absolute polarization error in general was less than 0.01 at angles forward of 110° and did not exceed 0.02 at larger angles.

II. EXPERIMENT AND RESULTS

The polarized source facility of the Rutherford Laboratory proton linear accelerator enabled accelerated proton beams of intensity about 2×10^9 protons sec^{-1}, with a polarization of 0.5, to be placed within a 0.7-cm circle on a target. The sign of the beam polarization could be inverted at the ion source, and scattering was recorded from targets of ^{58}Ni (200-keV thickness), ^{120}Sn (200-keV), and ^{208}Pb (400-keV). The target thicknesses were chosen with two criteria in mind: (1) to enable scattering from the first inelastic level to be well resolved from the elastic scattering at all angles, and (2) to ensure that the energy variation available on the accelerator was adequate to maintain the beam energy at the center of the target foil at 30.3 MeV for all target settings. This second criterion ensured that the polarization data obtained corresponded to the differential cross-section data of Ridley and Turner[4] to within ±100 keV.

The apparatus, described elsewhere,[6] was modified by the introduction of a new lid to the scattering chamber. This lid could be precisely oriented with respect to the beam axis and supported two NaI scintillation counters placed above the scattering plane at angles of ±18° relative to the beam axis. These were used to monitor the beam position on the target. The ratio of counting rates in these detectors changed by 10% for a lateral beam shift of about 0.5 mm on the target. This arrangement ensured that the over-all error in the mean scattering angle did not exceed ±0.25°.

The beam polarization was monitored continuously both at the exit of the accelerator, using the sampling polarimeter,[7] and after passing through the target, using the Birmingham University polarimeter.[8] The results of these two measurements showed excellent agreement on the basis of an efficiency of 0.655 for the sampling polarimeter and 0.57 at 15.7 MeV for the Birmingham University polarimeter. These efficiencies had been previously determined in independent absolute calibration experiments.

Detection of the scattered protons was made using four 5-mm-thick Li-drifted silicon detectors. The spin orientation of the beam was alternated frequently during a run at a given setting and the resulting spectra were routed into a pulse-height analyzer operating in a 8×128 mode. Four counting arrangements were used:

(1) At angles forward of 20°, strip targets 2 mm wide and normal to the beam were used, with detectors placed at $\pm\theta$ and $\pm(\theta+10)°$.

(2) At angles between 20 and 60°, foil targets were used normal to the beam with detectors at $\pm\theta$ and $\pm(\theta+10)°$.

(3) At angles between 60 and 125°, foil targets were used on a transmission setting with detectors at θ, $(\theta+10)$, $(\theta+20)$, and $(\theta+30)°$.

(4) At angles between 120 and 165°, foil targets were used on a reflection setting with detectors at θ, $(\theta+10)$, $(\theta+20)$, and $(\theta+30)°$.

The effective angular acceptance of the detectors varied between ±0.45 and ±0.82° with different targets and detector apertures. An accuracy in the measurements of polarizations of better than ±0.01 was attempted. This was, in general, achieved, with the exception of a few large-angle measurements at cross-section minima. The results, together with the errors, are listed in Table I.

Simultaneously with these measurements, relatively accurate data on the asymmetries in inelastic scattering to some 2^+ and 3^- excited states were obtained. These data together with some other similar data for ^{54,56}Fe are reported elsewhere.[9]

III. ANALYSIS AND DISCUSSION

The present data, along with the differential-cross-section data of Ridley and Turner,[4] have been analyzed using an optical model. Two versions of this model have been used: (1) the standard version in which all the terms of the potention are parametrized independently, and (2) the first-order folding model of Greenlees, Pyle, and Tang[2,3] in which the real parts of the potential are derived from the nuclear nucleon distributions via the two-body force.

The differential cross-section data of Ridley and Turner consists of approximately 80 points per element covering the angular range 4–162° in 2° steps. The present polarization data consists of approxi-

TABLE I. Polarization results for 30.3-MeV protons elastically scattered by ^{58}Ni, ^{120}Sn, and ^{208}Pb. The limits quoted on the angles represent the angular acceptance used for that particular measurement.

Angle (lab) (deg)	$P(\theta)$ ^{58}Ni	$P(\theta)$ ^{120}Sn	$P(\theta)$ ^{208}Pb	Angle (lab) (deg)	$P(\theta)$ ^{58}Ni	$P(\theta)$ ^{120}Sn	$P(\theta)$ ^{208}Pb
10 ±0.45	0.015 ±0.004	0.007 ±0.005	0.004 ±0.003	47.5 ±0.61	...	...	−0.080 ±0.013
12.5 ±0.45	−0.021 ±0.004	−0.004 ±0.005	0.014 ±0.003	50 ±0.82	−0.374 ±0.008	0.455 ±0.008	−0.214 ±0.008
15 ±0.45	−0.069 ±0.004	−0.003 ±0.004	0.014 ±0.004	55 ±0.82	−0.521 ±0.006	0.071 ±0.004	−0.253 ±0.009
17.5 ±0.45	−0.122 ±0.004	0.010 ±0.004	0.018 ±0.005	60 ±0.82	0.124 ±0.010	−0.245 ±0.005	0.246 ±0.003
20 ±0.61	−0.185 ±0.006	0.039 ±0.010	0.014 ±0.004	65 ±0.82	0.630 ±0.007	−0.677 ±0.006	0.314 ±0.004
22.5 ±0.61	−0.267 ±0.009	0.073 ±0.010	0.005 ±0.007	70 ±0.82	0.411 ±0.007	−0.550 ±0.011	−0.006 ±0.003
25 ±0.61	−0.401 ±0.011	0.089 ±0.006	−0.037 ±0.007	75 ±0.82	0.195 ±0.006	0.834 ±0.009	−0.372 ±0.005
26 ±0.45	−0.451 ±0.013	...	...	80 ±0.82	−0.046 ±0.008	0.446 ±0.008	−0.489 ±0.010
27 ±0.45	−0.568 ±0.017	...	...	85 ±0.82	−0.176 ±0.010	0.008 ±0.007	0.455 ±0.010
27.5 ±0.61	−0.392 ±0.017	0.044 ±0.007	−0.066 ±0.007	90 ±0.82	−0.005 ±0.008	−0.417 ±0.005	0.441 ±0.007
28 ±0.45	−0.221 ±0.018	...	...	95 ±0.82	0.569 ±0.006	−0.765 ±0.008	0.040 ±0.009
30[a]	0.813 ±0.013	−0.033 ±0.008	−0.075 ±0.003	100 ±0.82	0.898 ±0.007	0.314 ±0.013	−0.399 ±0.007
32 ±0.45	0.638 ±0.017	...	...	105 ±0.82	0.832 ±0.006	0.940 ±0.009	−0.723 ±0.008
32.5 ±0.45	...	...	−0.031 ±0.013	110 ±0.82	0.636 ±0.008	0.671 ±0.011	0.112 ±0.014
35[b]	0.301 ±0.006	−0.226 ±0.009	0.055 ±0.004	115 ±0.82	0.468 ±0.008	0.242 ±0.012	0.617 ±0.011
36 ±0.61	0.233 ±0.007	...	...	120 ±0.82	0.296 ±0.010	−0.192 ±0.013	0.301 ±0.015
37 ±0.45	0.153 ±0.020	...	...	125 ±0.82	0.183 ±0.009	−0.604 ±0.017	−0.178 ±0.012
37 ±0.61	0.172 ±0.006	...	...	130 ±0.82	0.182 ±0.015	0.028 ±0.040	−0.674 ±0.013
37.5 ±0.45	...	...	0.155 ±0.015	135 ±0.82	0.484 ±0.020	0.765 ±0.025	−0.490 ±0.027
38 ±0.61	0.126 ±0.005	...	...	140 ±0.82	0.906 ±0.015	0.954 ±0.022	0.701 ±0.022
40 ±0.82	0.043 ±0.006	−0.420 ±0.010	0.146 ±0.004	145 ±0.82	1.012 ±0.012	0.976 ±0.021	0.854 ±0.018
42 ±0.61	−0.051 ±0.006	...	...	150 ±0.82	0.983 ±0.011	0.680 ±0.033	0.512 ±0.021
42.5 ±0.61	...	...	0.115 ±0.012	155 ±0.82	0.865 ±0.010	0.036 ±0.027	−0.295 ±0.023
45 ±0.82	−0.140 ±0.008	0.204 ±0.014	0.012 ±0.006	160 ±0.82	0.561 ±0.014	−0.230 ±0.025	−0.989 ±0.020
47 ±0.61	−0.213 ±0.013	...	...	165 ±0.82	0.101 ±0.017	−0.320 ±0.019	−0.724 ±0.018

[a] ^{58}Ni ±0.45°; ^{120}Sn ±0.61°; ^{208}Pb ±0.82°.

[b] ^{58}Ni, ^{208}Pb ±0.82°; ^{120}Sn ±0.61°.

mately 40 points per element covering an angular range 10 to 165° in 2.5 and 5° steps. It seemed initially that about equal weight could be ascribed to the two sets of data by taking every other differential cross-section point of Ref. 4 (40 per element). The smoothness of the angular distributions of Ref. 4 and the closeness of the points ensured that no significant error was involved in this procedure. Reaction cross-section data at 28.5 MeV were also available[10] for the elements studied here. These data were not included explicitly in the analysis but the predictions obtained in all cases were always consistent with the errors in the experimental data.

A modified version of the computer code RAROMP[11] was used in these studies together with the University of Minnesota CDC-6600 computer. This code included both versions of the model used here and had an automatic search routine which varied the appropriate model parameters to find a minimum in χ^2 defined by

$$\chi^2 = \frac{1}{N}\sum_{i=1}^{N}\left(\frac{q_{\mathrm{th}}(\theta_i) - q_{\mathrm{exp}}(\theta_i)}{q_{\mathrm{error}}(\theta_i)}\right)^2, \qquad (1)$$

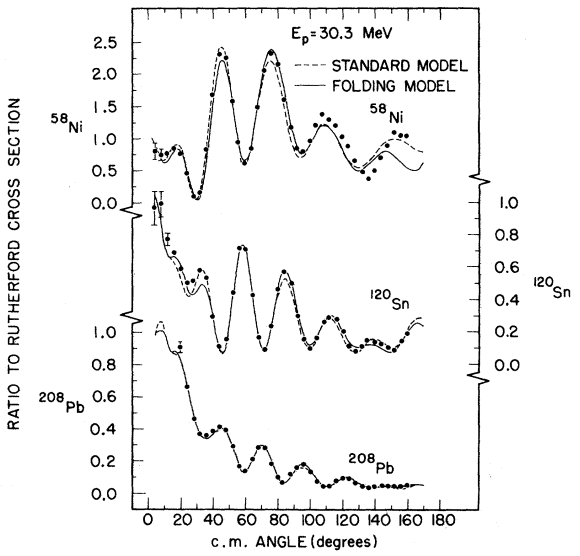

FIG. 1. Experimental differential cross-section data points, with errors, for the elastic scattering of 30.3-MeV protons (Ref. 4), together with predictions obtained from analyzing cross-section and polarization data using: (1) the standard optical model of Sec. III A (dashed line); and (2) the folding model of Sec. III B (solid line).

where $q_{th}(\theta_i)$ and $q_{exp}(\theta_i)$ are the theoretical and experimental quantities at scattering angle θ_i, respectively, and $q_{error}(\theta_i)$ is the associated experimental error. The experimental data were obtained using finite angular acceptances. In the case of the polarization data this angular range was as large as ±0.82° in some cases, and the angular distributions were such that this averaging could modify the shape somewhat. The program, therefore, took a weighted mean $\bar{P}(\theta)$ of the model predictions $P(\theta')$ over the angular range involved, $\Delta\theta$, using the expression

$$\bar{P}(\theta)=\int_{\theta-\Delta\theta/2}^{\theta+\Delta\theta/2}\sigma(\theta')P(\theta')d\theta' \Big/ \int_{\theta-\Delta\theta/2}^{\theta+\Delta\theta/2}\sigma(\theta')d(\theta') .$$

This value, $\bar{P}(\theta)$, was then used in Eq. (1) to determine a χ^2 minimum.

A. Standard Optical-Model Analysis

The potential used had the form

$$\begin{aligned} V(r) = &- V_{RS} f(r, r_R, a_R) - i W_V f(r, r_I, a_I) \\ &+ i 4 a_I W_S \frac{d}{dr} f(r, r_I, a_I) \\ &+ \left(\frac{\hbar}{m_\pi c}\right)^2 V_{so} \frac{1}{r}\frac{d}{dr} f(r, r_{so}, a_{so}) \vec{\sigma}\cdot\vec{l} + V_C(r), \end{aligned} \tag{2}$$

where

$$f(r, r_0, a_0) = [1 + e^{(r - r_0 A^{1/3})/a_0}]^{-1},$$

and $V_C(r)$ is the Coulomb potential due to a charge distribution $f(r, r_C, a_C)$ with $r_C = (1.106 + 1.05 \times 10^{-4} A)$ F and $a_C = 0.502$ F.[2,3] In this form, the model has ten adjustable parameters, V_{RS}, W_V, W_S, V_{so}, r_R, a_R, r_I, a_I, r_{so}, and a_{so}.

The data were analyzed in three ways: (1) using the cross-section and the polarization data; (2) using only the polarization data; and (3) using only the cross-section data. For procedure (3), the spin-orbit parameters, V_{so}, r_{so}, and a_{so}, were fixed at the values obtained in procedure (2) because of the insensitivity of the fitting to these parameters when only cross-section data were used. Except for this restriction in procedure (3), the search routine varied all parameters simultaneously. The parameters and χ^2 values obtained are listed in Table II. The model predictions, of procedure (1), together with the experimental points, are shown in Figs. 1 and 2.

Figures 1 and 2 show that the data are being well represented by the model. However, examination of Table II reveals the following features:

(a) For all three cases, the principal contribution to the χ^2 comes from the polarization data, so that these data play the major role in determining the parameters if it is included in the fitting procedure. The present polarization data are somewhat more accurate than the corresponding differential cross-section data. If the errors on both sets of data were comparable, the χ^2 contributions for each would be similar for the same model parameters; the model is therefore doing equally

TABLE II. Best-fit parameter sets obtained using the standard optical model for 30.3-MeV protons. Three combinations of experimental data were used: (1) elastic differential cross-section data (of Ref. 4) and the present polarization data ($\sigma+P$); (2) elastic polarization data only (P); and (3) elastic differential cross-section data only (σ). In case (3) the spin-orbit parameters were fixed at the values found in case (2). Typical errors in $\langle r^2\rangle_{RS}^{1/2}$ and J_{RS}/A are ±0.15 F and ±15 MeV F^3.

Element	^{58}Ni			^{120}Sn			^{208}Pb		
data analyzed	$\sigma+P$	P	σ	$\sigma+P$	P	σ	$\sigma+P$	P	σ
V_{RS} (MeV)	48.62	45.70	53.36	51.39	48.18	51.21	52.80	52.48	52.27
W_V (MeV)	3.27	0.75	3.37	2.62	0.01	2.34	2.29	2.63	1.90
W_S (MeV)	4.31	6.32	4.76	6.09	7.94	7.11	7.92	7.59	8.58
V_{so} (MeV)	6.16	5.78	5.78	6.25	5.71	5.71	5.96	5.71	5.71
r_R (F)	1.148	1.180	1.105	1.158	1.177	1.176	1.184	1.190	1.202
a_R (F)	0.748	0.715	0.770	0.772	0.756	0.706	0.689	0.674	0.676
r_I (F)	1.370	1.277	1.336	1.326	1.217	1.309	1.274	1.279	1.268
a_I (F)	0.550	0.717	0.551	0.696	0.956	0.679	0.746	0.703	0.752
r_{so} (F)	0.995	1.012	1.012	1.005	1.031	1.031	1.159	1.147	1.147
a_{so} (F)	0.612	0.597	0.597	0.728	0.684	0.684	0.599	0.585	0.585
$\langle r^2\rangle_{RS}^{1/2}$ (F)	4.43	4.42	4.38	5.27	5.30	5.20	6.01	6.01	6.06
J_{RS}/A (MeV F^3)	396	391	400	395	384	400	402	404	414
σ_R (mb)	1090	1172	1079	1675	1883	1641	1916	1857	1938
σ_R (expt) (mb)	1038 ± 43 at 28.5 MeV (Ref. 10)			1638 ± 68 at 28.5 MeV (Ref. 10)			1865 ±98 at 28.5 MeV (Ref. 10)		
χ^2_σ	15.5	...	5.2	8.1	...	2.9	3.8	...	1.0
χ^2_P	33.1	28.8	...	13.5	10.4	...	11.4	11.3	...
χ^2_T	24.7	28.8	5.2	10.7	10.4	2.9	7.8	11.3	1.0

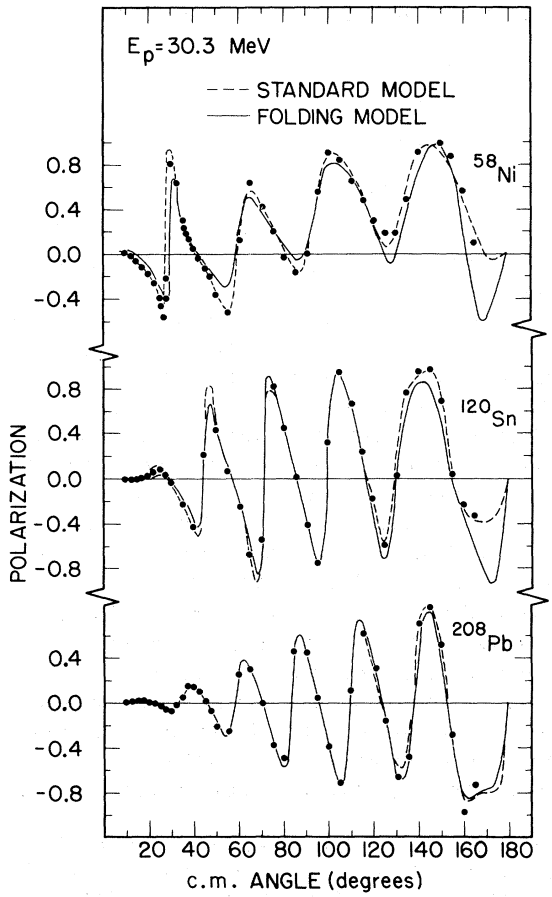

FIG. 2. Experimental polarization data points for the elastic scattering of 30.3-MeV polarized protons, together with predictions obtained from analyzing cross-section and polarization data using: (1) the standard optical model of Sec. III A (dashed line); and (2) the folding model of Sec. III B (solid line). The error bars are smaller than the size of the points plotted.

well in representing the two types of data. This is apparent in Figs. 1 and 2, where fits of similar visual quality are seen for corresponding data.

(b) The χ^2 values improve with increase in mass number of the target nucleus. Since the data for all cases were obtained with the same experimental arrangement, they are presumably of similar quality for each. Thus the increase in χ^2 for the lighter elements implies that the model is less satisfactory in these cases.

(c) Comparison of the parameters obtained using the three different combinations of data reveals very minor changes in the case of ^{208}Pb but significant changes for the other cases, with ^{58}Ni showing greater variations than ^{120}Sn. The constancy of the parameters obtained for ^{208}Pb whichever of the data are used, suggests that the data [$P(\theta)$ and $d\sigma/d\Omega$] are mutually consistent and testifies to the reliability of the measurements. This constancy also suggests that the model gives a good representation of the elastic interaction for heavy nuclei ($A \sim 200$). Since there is no reason to doubt the reliability of the ^{58}Ni and ^{120}Sn data compared with that of the ^{208}Pb data, the variations of parameters found for these elements, using the different analyses, can be attributed to shortcomings of the model description, which the mathematical freedom present in a ten-parameter representation attempts to rectify with varying results according to the data being fitted. The χ^2 value variations noted in (b) above, support this interpretation.

(d) The spin-orbit radius parameters found for ^{58}Ni and ^{120}Sn (~1.0 F) are appreciably lower than the value for ^{208}Pb (1.15 F). The ^{208}Pb value corresponds to a peaking of the spin-orbit interaction about 0.2 F outside the proton half-density point, whereas in the other cases the peak is about 0.5 F inside this point. Physically it is expected that the spin-orbit interaction will have a maximum where the nucleon density gradient is greatest. This point is very close to the proton half-density point for ^{58}Ni and probably at a slightly larger radial distance for ^{120}Sn and ^{208}Pb.[3]

B. Folding-Model Analysis

The model of Greenlees, Pyle, and Tang[2,3] obtains the real parts of the potential by folding the nuclear proton [$\rho_p(r)$] and neutron [$\rho_n(r)$] density distributions with the appropriate components of the nucleon-nucleon potential. This latter potential is taken to have the form

$$u_{0i} = u_d(r_{0i}) + u_\tau(r_{0i})\vec{\tau}_0\cdot\vec{\tau}_i + u_\sigma(r_{0i})\vec{\sigma}_0\cdot\vec{\sigma}_i + u_{\sigma\tau}(r_{0i})\vec{\sigma}_0\cdot\vec{\sigma}_i\vec{\tau}_0\cdot\vec{\tau}_i + [u_t(r_{0i}) + u_{t\tau}(r_{0i})\vec{\tau}_0\cdot\vec{\tau}_i]S_{12} + u_{ls}(r_{0i})\frac{1}{\hbar}[(\vec{r}_0 - \vec{r}_i)\times(\vec{p}_0 - \vec{p}_i)\cdot(\vec{\sigma}_0 + \vec{\sigma}_i)]\,. \quad (3)$$

Neglecting target polarization and antisymmetrization effects, the real effective interaction potential for protons can be written as

$$U_0 = U_R + U_S + U_{so}\,, \quad (4)$$

where

$$U_R = \int [\rho_n(\vec{r}) + \rho_p(\vec{r})]u_d(|\vec{r} - \vec{r}_0|)\,d\vec{r}\,, \quad (5)$$

$$U_S = \int [\rho_p(\vec{r}) - \rho_n(\vec{r})]u_\tau(|\vec{r} - \vec{r}_0|)\,d\vec{r}\,, \quad (6)$$

and

$$U_{so} = \left\{ -\frac{1}{\hbar}\sum_{n=1}^{\infty}\frac{4\pi}{(2n+1)!}\frac{2n}{r_0}\frac{d}{dr_0}\left[\frac{2(n-1)}{r_0}\times\frac{d^{2n-3}}{dr_0^{2n-3}}(\rho_n+\rho_p) + \frac{d^{2n-2}}{dr_0^{2n-2}}(\rho_n+\rho_p)\right] \times\int_0^\infty u_{ls}(\eta)\,\eta^{2n+2}\,d\eta\right\}\vec{l}_0\cdot\vec{\sigma}_0\,. \quad (7)$$

A previous paper[3] concluded that these two-body force components should be taken from an analysis of low-energy nucleon-nucleon data and used for u_d a Gaussian form with msr 4.27 F^2; for $-u_\tau$, $0.48u_d$; and for u_{ls}, a Yukawa form with msr 0.5 F^2. The strengths of u_d and u_{ls} were left as adjustable parameters. This procedure gave good fits to the 30.3-MeV proton elastic differential cross sections of Ref. 4. However, the analysis of two-body data used to obtain u_d included both singlet and triplet components of different ranges. The 4.27 F^2 was an appropriate mean of these. In the present analysis the singlet and triplet folding is included explicitly. Assuming a Serber mixture it follows that

$$u_d = \tfrac{3}{16}(V_t + V_s) \tag{8}$$

and

$$u_\tau = -\tfrac{1}{16}(3V_t - V_s), \tag{9}$$

where V_t and V_s are the triplet and singlet nucleon-nucleon interactions in the even-l states. An analysis of low-energy (<100-MeV lab) nucleon-nucleon data by Reichstein and Tang[12] gave

$$V_t = -V_{0t}\, e^{-K_t r^2} \tag{10}$$

and

$$V_s = -V_{0s}\, e^{-K_s r^2} \tag{11}$$

with $V_{0t} = 66.92$ MeV, $V_{0s} = 29.05$ MeV, $K_t = 0.415$ F^{-2}, and $K_s = 0.292$ F^{-2}. The ratio $-(u_\tau/u_d)$ is now radially dependent. A phenomenological imaginary term is added to U_0 to represent interactions other than elastic scattering. This term has the same form as in Eq. (2).

Repeating the analysis of Ref. 3 with this more complete form of the model produced negligible changes in the conclusions.

The interaction potential used here may be written as

$$V(r) = V_C(r) - V_{RS}\frac{I_{nt} + \frac{1}{3}\alpha(I_{ns} + 2I_{ps})}{(I_{nt} + I_{pt}) + \alpha(I_{ns} + I_{ps})} - i\,W_v f_I(r, r_I, a_I) + i\,W_S 4a_I \frac{d}{dr} f_I(r, r_I, a_I) - V_{so}\, I_{so}(r)\,\vec{\sigma}\cdot\vec{l}\,, \tag{12}$$

where $V_C(r)$ is the Coulomb potential as used in Sec. III A and,

$$I_{ij}(r) = \int f_i(\vec{\eta})\, g_j(|\vec{\eta} - \vec{r}|)\, d\vec{\eta}\,,$$

$$\frac{\rho_i(r)}{\rho_{i0}} = f_i(r) = \left[1 + e^{(r - r_i A^{1/3})/a_i}\right]^{-1},$$

$$g_j(r) = e^{-K_j r^2},$$

$i = p$, for proton, n, for neutron;

$j = t$, for triplet, s, for singlet;

$K_t = 0.415$ F^{-2};

$K_s = 0.292$ F^{-2};

$\alpha = V_{0s}/V_{0t} = 0.4341$.

The spin-orbit term I_{so} is obtained as described in Ref. 3 [Eq. (15)] using a Yukawa form for u_{ls} with a msr of 0.5 F^{-2}.

The proton distribution parameters are obtained from the measured charge distributions by unfolding the finite proton size giving[2,3] $r_p = (1.106 + 1.05 \times 10^{-4}A)$ F and $a_p = 0.454$ F.[2,3] This leaves eight adjustable parameters, which are varied simultaneously to find a minimum in χ^2 as defined by Eq. (1). The parameters are r_n, a_n, r_I, a_I, V_{RS}, V_{so}, W_V, and W_S, and the best-fit values obtained are listed in Table III. The corresponding model predictions are included in Figs. 1 and 2.

As in the case of the analysis of Sec. III A, the principal contribution to the χ^2 values of Table III comes from the polarization data; this can once again be ascribed to the greater accuracy of these points rather than to any inherent difference in the model representation. The χ^2 values improve with increasing target mass number, and for the heavi-

TABLE III. Best-fit parameters using the singlet and triplet two-body potentials as outlined in the text. The present 30.3-MeV proton polarization data, together with the differential cross-section data of Ref. 4 were analyzed simultaneously. The normalization of the spin-orbit term is different from that used in Table II. A strength here of about 2000 MeV corresponds to a strength of 6 MeV in Table II. Typical errors in $\langle r^2\rangle_n^{1/2}$, $\langle r^2\rangle_{RS}^{1/2}$, and J_{RS}/A are ±0.2 F, ±0.15 F, and ±15 MeV F^3. The experimental reaction cross sections quoted are from Ref. 10 for a proton energy of 28.5 MeV.

Element	^{58}Ni	^{120}Sn	^{208}Pb
V_{RS} (MeV)	57.39	54.24	51.30
W_V (MeV)	5.71	3.69	1.15
W_S (MeV)	2.85	5.99	11.24
V_{so} (MeV)	1620	1578	1729
r_I (F)	1.403	1.320	1.260
a_I (F)	0.417	0.651	0.668
r_n (F)	1.133	1.154	1.210
a_n (F)	0.528	0.540	0.453
$\langle r^2\rangle_{RS}^{1/2}$ (F)	4.38	5.21	6.09
J_{RS}/A (MeV F^3)	400	396	405
σ_R (mb)	1067	1652	1900
σ_R (expt) (mb)	1038 ± 43	1638 ± 68	1865 ± 98
χ^2_σ	24.0	11.7	3.8
χ^2_P	175.0	40.8	17.2
χ^2_T	103.5	25.5	10.9
$\langle r^2\rangle_n^{1/2}$ (F)	3.92	4.84	5.80
$\langle r^2\rangle_n^{1/2} - \langle r^2\rangle_p^{1/2}$ (F)	0.18	0.25	0.36

est nucleus (^{208}Pb), are similar to those obtained with the ten-parameter model. However, for ^{120}Sn, and more so for ^{58}Ni, the representation of the data is less satisfactory with the folding model, the χ^2 values being two to four times greater, respectively, and the visual quality of the fits is noticeably worsened. The reason for this is readily apparent. Since the folding procedures used in this section, to a good approximation, modify only the fall-off of the potential form factors relative to the nucleon distributions, the halfway point of the real central potential and the maximum of the spin-orbit potential are located very close to the nucleon half-density radius. This corresponds in the standard treatment, with independent geometries for these two terms, to imposing a constraint of $r_R = r_{so}$. Table II shows that, for ^{208}Pb, r_{so} is close to r_R (1.16 and 1.18 F), so that imposing such a constraint does not appreciably change the quality of the fit. For ^{58}Ni and ^{120}Sn, Table II shows r_{so} to be appreciably less than r_R in both cases (1.0 compared to 1.15 F). It is reasonable, therefore, to attribute the improvement in fit achieved with the standard model for these cases to the uncoupling of the real central and spin-orbit geometries. The improvement is clearly visible in Fig. 2 for ^{58}Ni and ^{120}Sn. However, as noted in Sec. III A, the model cannot do as well for the lighter elements as it does for ^{208}Pb, even in the ten-parameter version, and the peaking of the spin-orbit term about 0.5 F inside the nucleon half-density point and in a region of nearly constant density is difficult to understand physically. It seems probable, therefore, that the improved fitting achieved for Ni and Sn with the standard model of Sec. III A compared with the folding model of the present section is more a result of increased mathematical freedom rather than a basically better representation of the interaction. Additional evidence for this conjecture comes from a coupled-channel analysis of the inelastic cross sections and asymmetries measured in conjunction with the present elastic polarization data; this has been reported separately.[9] A significant finding of this analysis, which included data for 2^+ and 3^- states of ^{54,56}Fe, ^{58}Ni, ^{120}Sn, and ^{208}Pb, was that for medium-weight elements, much improved asymmetry fits were found using optical-model parameters, obtained from an analysis of elastic scattering data, including the constraint $r_R = r_{so}$; this implies that such sets are physically more acceptable. It is suggested that the model, in either version, gives a good representation of the elastic interaction for heavy nuclei (^{208}Pb) but is over simplified for lighter systems (^{120}Sn and ^{58}Ni). This could possibly be represented by an l dependence of the potential which would be expected to be most marked for low l values, which in turn play a relatively more important role the smaller the nucleus.

The present work reproduces some features noted in the analysis of Ref. 3, which included 30.3-MeV differential cross-section data and a very small amount of polarization data, and also used only a single range for u_d. The volume integral (J_{RS}) and mean square radius ($\langle r^2 \rangle_{RS}$) of the real central potential ($U_R + U_S$) are well defined and insensitive either to the detailed form of the potential used or to the type of data analyzed [$d\sigma/d\Omega$ or $P(\theta)$]; this can be seen in Tables II and III. Furthermore, the volume integral per nucleon of the real central potential (J_{RS}/A), is independent of A [and $(N-Z)/A$] to within the accuracy achieved. This latter result was unexpected, since with protons the strength of the total interaction per nucleon (here measured by J_{RS}/A) would be expected to increase as the nuclear neutron-proton ratio increased. This result is consistent with the suggestion made above that the model is a good representation of the interaction for heavier (larger) nuclei but oversimplified for lighter (smaller) nuclei. The neutron-proton rms radius differences found here are slightly greater than were found in Ref. 3; however, the increase is no greater than the errors in the determinations ($\sim \pm 0.2$ F).

IV. CONCLUSIONS

An optical-model analysis has been presented of relatively accurate differential cross-section and polarization data for the elastic scattering of 30.3-MeV protons from ^{58}Ni, ^{120}Sn, and ^{208}Pb. Two forms of the model have been used, the standard ten-parameter form with independent geometries and the eight-parameter folding version of Greenlees, Pyle, and Tang[2,3] with the inclusion of singlet and triplet two-body forces. In the case of ^{208}Pb, a good representation of the data is obtained and the fits with the two procedures are visually equivalent. Both versions of the model are less satisfactory for ^{120}Sn and ^{58}Ni. In these latter cases, the standard model achieves a better representation than the folding model. This feature is associated with the additional freedom in the spin-orbit radius parameter allowed in the standard version, which in the case of Sn and Ni produces a peaking of the spin-orbit potential about 0.5 F inside the half-density point for these nuclei.

It is suggested that an optical-model description of the type normally used for elastic scattering data is satisfactory only for heavy nuclei ($A \sim 200$), and that for smaller systems some second-order processes are playing a non-negligible role. The main pieces of evidence for this are:

(1) larger χ^2 values for smaller nuclei, with data

of comparable quality;
(2) variations in parameters for smaller nuclei dependent upon whether cross-section or polarization data, or both, are analyzed;
(3) peaking of the spin-orbit interaction in a region of relatively constant nuclear density for the smaller nuclei when the real central and spin-orbit radius parameters are allowed to vary independently;
(4) improved fits to inelastic data for medium-weight nuclei when the optical-model parameters involved have the same real central and spin-orbit radius parameters;
(5) absence of an isospin $[(N-Z)/A]$ dependence of the real-central-potential volume integrals. To test this suggestion additional accurate and extensive data will be needed, together with an investigation of the second-order processes arising from consideration of polarization and antisymmetrization effects which were neglected in the folding model used here.

Modifications to the central terms, due to second-order effects, have been semiquantitatively examined by Drell[13] and found to be small.[14] Modifications to the spin-orbit potential due to such effects have not been reported for cases such as those studied here; however, some preliminary calculations on the proton-α system[15] have indicated that the effects of antisymmetrization on the spin-orbit potential are quite significant in this light system. It is possible that a similar study for the heavier systems considered here might explain the present results.

ACKNOWLEDGMENTS

One of us (G.W.G.) wishes to acknowledge the hospitality and generous cooperation of the Rutherford High Energy Laboratory during his stay there on leave from the University of Minnesota. The services of the University of Minnesota Numerical Analysis Center are also gratefully acknowledged.

---

†Work supported in part by the U. S. Atomic Energy Commission, publication Report No. COO-1265-88.

[1]F. D. Becchetti, Jr., and G. W. Greenlees, Phys. Rev. 182, 1190 (1969).
[2]G. W. Greenlees, G. J. Pyle, and Y. C. Tang, Phys. Rev. 171, 1115 (1968).
[3]G. W. Greenlees, W. Makofske, and G. J. Pyle, Phys. Rev. C 1, 1145 (1970).
[4]B. W. Ridley and J. F. Turner, Nucl. Phys. 58, 497 (1964).
[5]R. M. Craig, J. C. Dore, G. W. Greenlees, J. S. Lilley, J. Lowe, and P. C. Rowe, Nucl. Phys. 58, 575 (1964).
[6]D. J. Baugh, M. J. Kenny, J. Lowe, D. L. Watson, and H. Wojciechowski, Nucl. Phys. A99, 203 (1967).
[7]N. S. Chant, Rutherford High Energy Laboratory Progress Report No. RHEL/R 156 (unpublished), p. 160.
[8]R. M. Craig, J. C. Dore, G. W. Greenlees, J. S. Lilley, J. Lowe, and P. C. Rowe, Nucl. Instr. Methods 30, 268 (1964).
[9]O. Karban, P. D. Greaves, V. Hnizdo, J. Lowe, and G. W. Greenlees, Nucl. Phys. A147, 461 (1970).
[10]J. F. Turner, B. W. Ridley, P. E. Cavanagh, G. A. Gard, and A. G. Hardacre, Nucl. Phys. 58, 509 (1964).
[11]G. J. Pyle, John H. Williams Laboratory of Nuclear Physics Report No. COO-1265-64 (unpublished).
[12]I. Reichstein and Y. C. Tang, Nucl. Phys. A139, 144 (1969).
[13]S. D. Drell, Phys. Rev. 100, 97 (1955).
[14]A more quantitative calculation of second-order effects in the α-α system has been reported by A. Herzenberg and E. J. Squires, Nucl. Phys. 19, 280 (1960).
[15]Y. C. Tang, private communication.